# FLUID FLOW THROUGH POROUS MEDIA WITH DUAL SCALE POROSITY

*A.G. Andersson[1], L.G. Westerberg[1], T.D. Papathanasiou[2], T.S. Lundström[1]*

[1]Division of Fluid Mechanics, Department of Applied Physics and Mechanical Engineering
Luleå University of Technology, SE-971 87 Luleå, Sweden

[2]Department of Chemical Engineering, University of South Carolina, Columbia, SC 29208

## ABSTRACT
Flow in two scale porous media takes place in many applications, including advanced composites manufacturing. Knowledge of this flow is of general importance and is crucial for filtration mechanisms when functional filler-particles are added to the liquid resin impregnating the fibrous preform. Means to model and experimentally visualise such flows are here investigated. In particular simulations performed with computational fluid dynamics and the boundary element method are augmented by micro particle image velocimetry (μPIV) in a model geometry.

## INTRODUCTION
The flow through porous media is of importance in many applications including composites manufacturing, paper making and drying of iron ore pellets. In general, prediction of porous media flow is straight-forward, as it is governed by Darcy's law. However when it comes to fluid flow in dual-scale porous media, which is the case for all examples mentioned above, the detailed flow becomes more complex. In fibre reinforced composite materials being the material in focus in this paper, the dual scale porosity is formed when the fibres are collected in bundles (Parnas et al., 1994). The flow of liquid resin during impregnation therefore takes place on two scales, the fibre scale 10 μm and the fibre bundle scale 100 μm as exemplified in Fig.1. The result of this is that the velocity of the liquid resin in the inter bundle channels is orders of magnitude higher than the velocity within the bundles themselves. There is also a natural variation in the distribution of the fibres within a bundle implying that the velocity can vary a lot within a fibre bundle, as well, see Fig.1. The fibre bundles in their turn are often assembled in an organised way by weaving or stitching techniques but their exact positions will deviate from a perfect pattern due to statistical variations and manufacturing induced flaws. For this reason, the velocity in the inter bundles channels will also be spatially variable. It is therefore not straight-forward how to model the flows taking place during impregnation of fibre reinforcements. One way of doing this is to use Computational Fluid Dynamics (CFD) in order to calculate the permeability of cells with a typical geometry as done in Nordlund et al. (2006). The cells can then be connected to form a network for which the total permeability can be computed (Lundström et. al., 2004). In such computations a number of approximations are introduced, one of which is the value of the permeability within a fibre bundle. In Nordlund et al. (2006) this was approximated using the formulas suggested by Gebart (1992) for flow along and perpendicular to regular fibre arrays according to

$$K_{//} = \frac{8}{C}\frac{(1-f)^3}{f^2}R^2 \tag{1}$$

$$K_{\perp} = C\left(\sqrt{\frac{f_{\max}}{f}}-1\right)^{5/2}R^2 \tag{2}$$

where $f$ is the bundle fibre volume fraction, C a constant being close to unity and $R$ the fibre radius. The constant $C$ and the maximum fibre volume fraction $f_{max}$ are both strongly dependent on the arrangement of the fibres. Obviously, this approach will result in a homogenous flow through the fibre bundle, and this, in some cases might be a too crude an assumption. To summarize, CFD can be used to simulate rather complex 3D structures on the fibre bundle scale but the specific value of the permeability within the fibre bundles must be assumed.

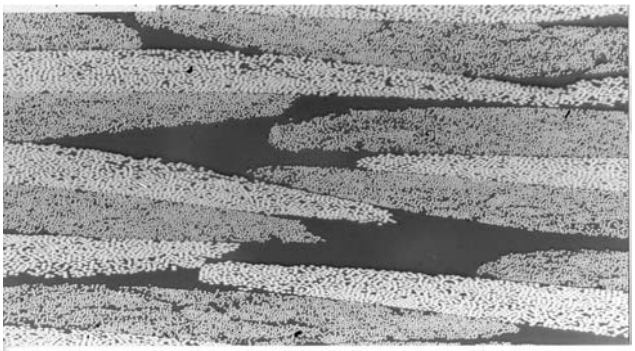

Fig.1. Cross-section of a moulded fibre reinforced composite material. The white and light grey areas are fibres in different directions while the dark grey area denotes the solidified resin. The diameter of the fibres is about 5 μm.

Another way of predicting the flow through and around fibre bundles is to apply the Boundary Element Method (BEM) and resolve every fibre within the bundles (Chen and Papathanasiou, 2006, 2008). With such an approach the small scale has a potential to be perfectly modelled but it becomes very difficult to model 3D effects on the fibre bundle scale which can be done with CFD. In this paper we apply both methods to the problem at hand.

A third possible route to study this flow is to do detailed flow visualisations. When doing experiments on geometries of sub-millimetre scale, non-intrusive methods are preferred. One such optical evaluation method is Particle Image Velocimetry (PIV) with which the flow can be visualized and with which also quantitative measurements of instantaneous velocity fields can be performed (Raffel et al. (1998)). PIV or,

when applied on a micro scale, μPIV has been used to investigate flows through rectangular arrays of circular fibres (Zhong et al., 2006 and Agelinchaab et al., 2006); comparing results between experiments and theory which showed good agreement. Hence, μPIV will here be applied to study the flow in a dual scale model geometry consisting of an array of parallel fibres placed in a cavity. Prior to this results from simulations on a CFD-model of the same set-up will be presented and the boundary element method will be introduced.

## CFD MODELLING OF POROUS DOMAIN

A computational model of an existing experimental flow cell was created using the commercial software CFX-11 from ANSYS and structured numerical grids were created in ICEM-CFD11, also from ANSYS. The geometry consists of an inlet pipe with $R$ = 0.6 mm which leads to a 1.6 mm wide slit designed to limit three dimensional flow effects. The slit in turn is connected to the main channel, which is a rectangular box with dimensions 5.3 x 7 x 7 mm$^3$, see Fig.2. The main channel has a porous region, in reality consisting of a 4 x 4 mm$^2$ array of fibres, whose length, in the direction perpendicular to the direction of the bulk flow, takes up the entire channel depth. The fibre volume density is set to about 40 % which is the same as for the experimental cell. Open regions are left around the fibre array to allow different flow phenomena to be investigated.

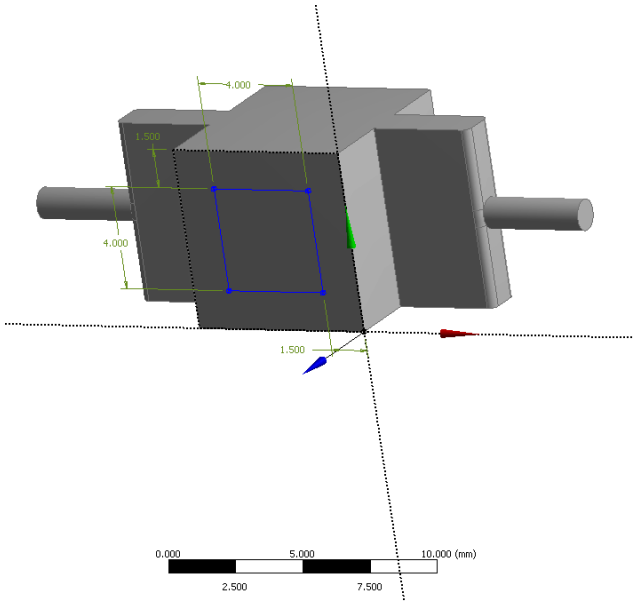


Fig.2. Geometry of investigated cell.

The fibre bundle was modelled as a porous domain with permeability $K_\perp$ given by Eq.(2) with the constant C and $f_{max}$ corresponding to a hexagonal fibre arrangement. The flow rate at the inlet was set to 5.56e-9 m$^3$/s and the outlet had an average static pressure set to 0 Pa. A no slip condition was set to all the walls.

The advection scheme used in the simulations was Specified Blend factor = 1, which is a second order accurate discretisation of the advection term in the momentum equations. As convergence criterion it was decided that the RMS residuals should all be below $10^{-6}$, which according to ANSYS is sufficient even for geometrically sensitive problems. A mesh dependency study was performed to ensure grid independent solutions were achieved.

## RESULTS OF CFD

It is observed that the surrounding flow affects the velocity inside the bundle, resulting in a boundary layer flow within the porous medium with higher velocity near the edges, see Fig.3 showing a contour plot of the velocity field.

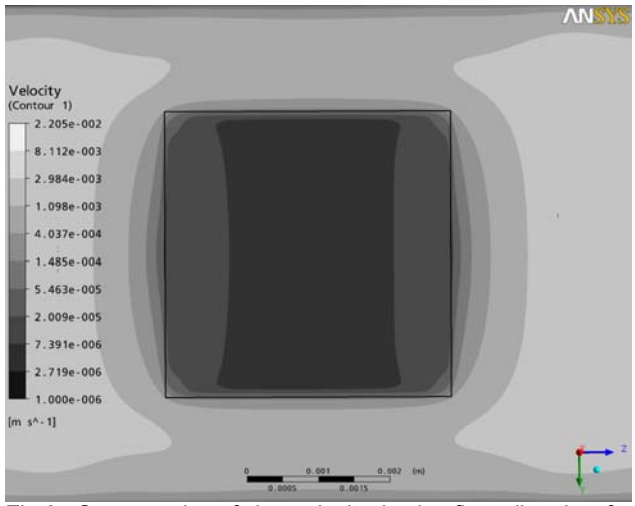


Fig.3. Contour plot of the velocity in the flow direction for fibre bundle and surrounding flow in the symmetry plane.

Different values of the permeabilities, 100 times greater and 1000 times greater than for the experimental cell, were also investigated,, see Fig.4. showing the velocity profile in the centre of the channel. The porous region is located between Y = ±0.002m.

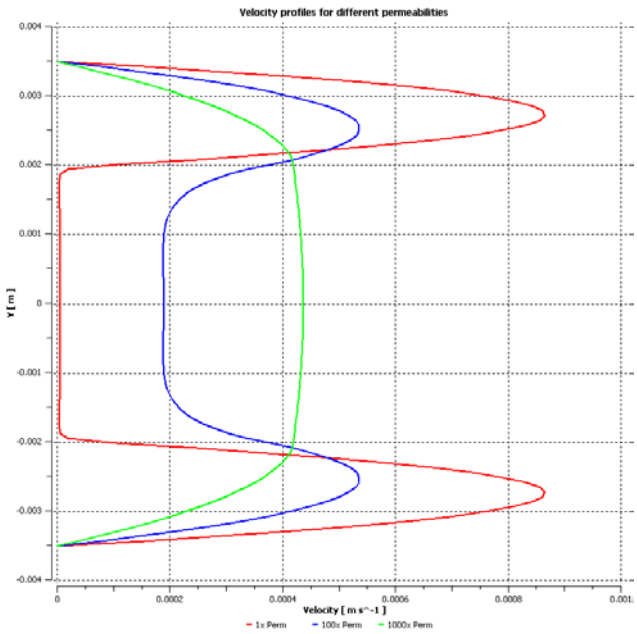


Fig.4. Velocity profiles for different permeabilities in the center of the bundle in the symmetry plane.

It can be observed that with increased permeability the difference in velocity between the bundle flow and the open channel flow is decreasing, just as expected. The boundary layer effect on the flow also affects a larger portion of the fibre bundle. For permeability 1000 times larger than the original, the velocity inside the bundle is even larger than in the surrounding flow.

**BEM MODELLING OF POROUS DOMAIN**

The next approach is to use the Boundary Element Method (BEM) to model Stokes flow through dual-scale porous media (unit cells), each containing one bundle of fibres. The axes of the fibres are oriented perpendicular to the bulk flow. Such dual-scale systems are characterized by their inter-tow porosity $\varphi_i$ associated with the interstitial space between fibre tows, the porosity of the intra-tow space $\varphi_t$, $\varphi_t$ = 1-*f*, the number of fibres in the tow $N_f$, the fibre radius *R* and the tow axis ratio $\lambda$. In addition, a microstructural parameter needs to included, to account for the degree of uniformity in the intra-tow fibre placement. This parameter is chosen here to be the mean nearest inter-fibre spacing, $\delta_1$. It has been established (Chen and Papathanasiou, 2006, 2008) that, as the degree of heterogeneity in the fibre distribution increases, $\delta_1$ decreases. These fibre distributions can be generated by a Monte Carlo (MC) process, in which the minimum inter-fibre spacing ($\delta_{min}$) is introduced to prevent adjacent fibres from overlapping (Chen & Papathanasiou, 2006). A uniform fibre distribution is generated by assigning a large value to $\delta_{min}$, while less uniform fibre distributions are formed by assigning progressively smaller $\delta_{min}$ values. The minimum achievable value of $\delta_1$ is zero, corresponding to the state at which all fibres are touching each other to form an impenetrable cluster, while the maximum $\delta_1$ equals the inter-fibre spacing of a hexagonal array - this is a function of porosity only.

The linear system of equations to be solved in the BEM is derived from the discretization of the boundary integral equation (Brebbia and Dominguez, 1989) using appropriate shape functions (quadratic in this study) for the geometry, the velocities $\boldsymbol{u}$ and the tractions $\boldsymbol{t}$ - the latter are related to the total stress tensor *T* by

$$t_j = T_{ij} n_i \tag{3}$$

where $n_i$ is the outward unit normal vector on each node. The boundary conditions used are those of symmetry on the two horizontal boundaries of the unit cell, Fig.5. and of unidirectional flow and of a constant total pressure drop along the two vertical boundaries. On the surface of each fibre in the bundle, no-slip conditions are applied. After imposing the boundary conditions, a linear system of equations,

$$\mathbf{A}\mathbf{x} = \mathbf{b} \tag{4}$$

result, in which the matrix $\boldsymbol{A}$ is full and non-symmetric. Solution can be obtained using either a direct method such as the L-U decomposition or an iterative method such as the Generalized Minimum RESidual (GMRES) method. The current solution strategy is to use a parallel LU solver from the ScaLapack library (Blackford et al., 1997) and an in-house parallel code for the formation of the matrix $\boldsymbol{A}$ and for post-processing, using MPI. A typical simulation, containing ~50,000 unknowns, takes about an hour to complete using 64 nodes in a commodity Dell cluster.

**RESULTS OF BEM AND COMPARISONS TO CFD**

A look into the detailed flow pattern within a fibre bundle surrounded by a flowing fluid helps gain some physical insight into the problem. It is accepted that in a dual-scale flow, such as the one studied here, there will be a boundary layer flow within the porous medium in which the velocity is higher than the Darcy velocity prevailing within the porous medium. So far the CFD results are in agreement with the BEM, cf. Fig.3 and Fig.5. This boundary layer flow is, however, largely affected by the structure of fluid-tow interface (Larson and Higdon, 1987). Fig.5. shows the contours of flow speed calculated for two contrasting intra-tow fibre distributions under the conditions: $\varphi_i$ = 0.5, $\varphi_t$ = 0.5, $\lambda$ = 2 and $N_f$ = 500. It can be seen that more fluid penetrates into the non-uniform fibre tow due to the large pores along its perimeter. In the flow field observed inside the non-uniform fibre tow, the regions of faster flow also extend further to the interior of the tow than their counterparts in the flow field caused by the uniform fibre tow. These results suggest that the boundary layer flow in a non-uniform fibre tow is larger than that in a uniform tow.

At this point, it is, therefore, instructive to compare the permeability predictions $K_p$ of the dual-scale approach illustrated in Fig.5. to those of existing models in which the fibre bundle is considered to be a porous medium of some effective porosity $K_t$ for instance given by Eq. (1) or (2). Since the actual value of $K_t$ is generally unknown, the usual practice is to assign to it the value corresponding to a hexagonal or square array. In Fig.6. we compare the predictions of the Phelan-Wise model (Phelan and Wise, 1996) with those obtained by the BEM. Our numerical predictions, based on heterogeneous fibre tows, are generally different from model predictions based on the assumption of a $K_t$ corresponding to a square (SQ in Fig.6.) or hexagonal (HEX) intra-tow fibre packing. This is especially true at larger values of the intra-tow porosity $\varphi_t$, where intra-tow flow will be important. Based on these comparisons, it is clear that substitution of the permeability of a regularly packed fibre array into the Phelan-Wise model would not produce an accurate estimate of the overall permeability or provide a satisfactory explanation for the permeability variation observed in experiments. The inverse approach, namely the experimental measurement of the permeability of systems similar to Fig.5. and the back-calculation of $K_t$ by fitting the results of the Phelan & Wise model would be more suitable. Since the permeability of a dual-porosity system with irregular intra-tow fibre placement is higher than the permeability of a system with uniform intra-tow fibre placement (the latter being closer to the hexagonal arrays), it would appear that the “effective” $K_t$ of the

latter would be smaller. This is the opposite to what analysis of random (but un-clustered) fibre arrays has shown (Chen and Papathanasiou, 2008), where it was concluded that deviation from the uniform array results in a reduction of the effective permeability. The source for this difference is to be found in the microscopic details of the flow in the perimeter of the fibre bundle, and we are working in this direction.

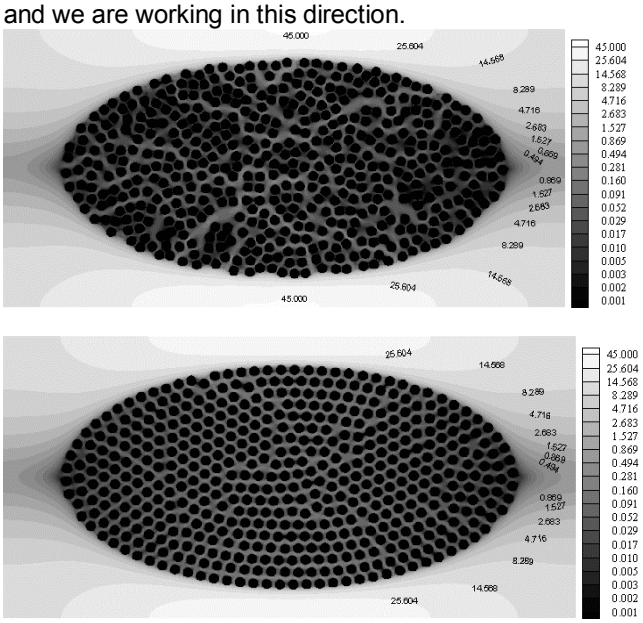

Fig.5. Contours of flow speed in two systems having different intra-tow fibre distributions. (top) $\delta_1/R=0.05$, (bottom) $\delta_1/R=0.295$. The geometrical parameters of the two systems are otherwise the same ($\varphi_i=0.5$, $\varphi_t=0.7$, $N_f=500$ and $\lambda=2$).

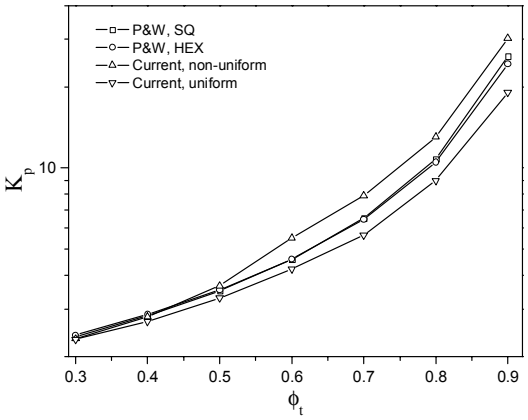


Fig.6. Comparison of the predictions of the Phelan-Wise model (P&W) with numerical results for $\varphi_i=0.40$. The other conditions are $\lambda=1$, $N_f=500$ and $R=1.0$ for all. The value of the ratio $\delta_1/R$ is 0.05 and 0.295, for the "non-uniform" and the "uniform" intra-tow packings, respectively.

## EXPERIMENTAL SET-UP

Experiments were conducted on the flow cell of Fig.7. The dimensions and its key geometrical/flow features are the same as in the model used in the ANSYS simulations.

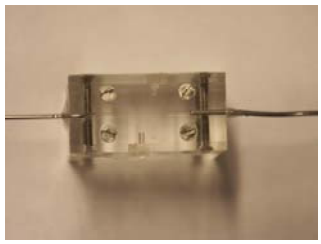

Fig.7. Flow cell, showing the inlet/outlet pipes.

The porous region of the channel consists of borosilicate glass fibre rods which can be arranged in different formations, perpendicular to the bulk flow direction. The rods have a radius of $R$ = 150 μm. The first investigation was made on a rectangular fibre array with relatively low solid volume fraction. The second investigation was made on a much denser hexagonally arranged array with a fibre volume density of about 40 %, see Fig.8.

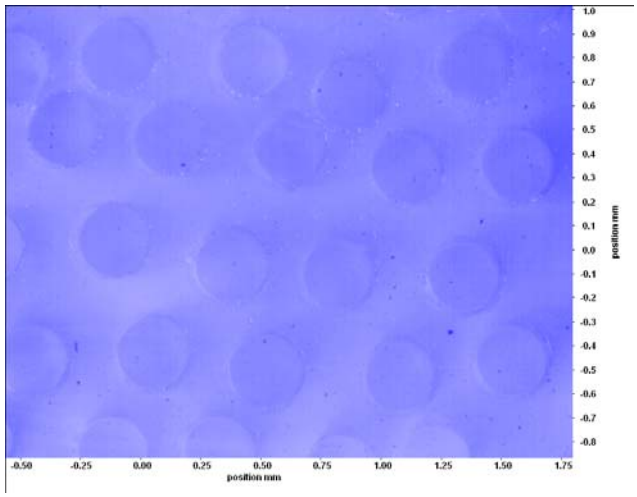


Fig.8. Image of a section of the fibre array obtained using 10x magnification. The bulk flow is in the direction perpendicular to the fibre axes.

In typical μPIV the flow is seeded with fluorescent particles and illuminated by a light source before it is imaged through a microscope into a CCD camera, see Fig.9.

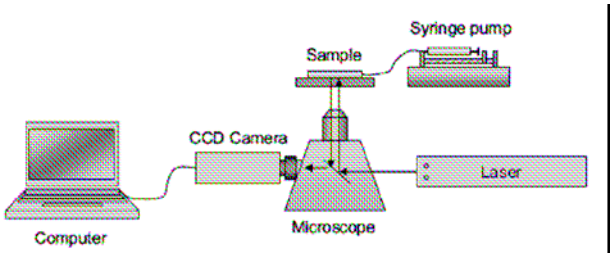


Fig. 9. Experimental setup

A pulsed ND:YAG laser from Litron Lasers emitting light with a wavelength of 532 nm was used as a light source in the experiments. The choice of fluid for the experiments was paraffin oil since it has a refraction index that is close to the refraction index of the glass walls of the channel. The fluorescent particles used were 10.2±0.17μm Rhodamine B particles from Microparticles GmbH. In order to get good results a homogenous distribution of particles in the fluid is needed. One of the

major problems when dealing with mixing in the particles to the fluid is avoiding adding of air bubbles to the fluid. The procedure that seemed to give the best quality mixture was to extract as much air as possible before any particles was added to the fluid. This was done by leaving the clear fluid in a vacuum pump until all air bubbles were removed. The particles were then carefully added. Stirring was not considered a good alternative for mixing since too much air was entrapped in the oil. Instead the container with the oil and the particles was placed in a sonic bath for a few minutes. After this the fluid was put it in vacuum once more in order to remove residual air. In order to get a constant velocity of the flow into the channel, a KDS Model 100 Series syringe pump was used with the volume flow rate set to 20ml/h.

A good signal-to-noise ratio was achieved by having as few particles as possible while still making it possible to do measurements (Meinhart et al. 2000). A lower particle concentration means that is difficult to get a complete velocity field from every picture pair. In order to get sufficient data for the velocity field, a method called sum of correlation was used. Sum of correlation uses information from several images that all contain partial data to get a complete description of the velocity field.

The flow in the channel is three dimensional while the μ-PIV set-up used gives only the two planar components of the velocity field. It was therefore desired to measure the velocity field where the out-of-plane component of the flow had as little influence as possible, in other words in the centre of the channel.

Since the permeability is much lower in the fibre bundle, the flow there is significantly slower. This implies that cross-correlation of the movement of the particle inside and outside of the porous domain at the same time is tricky. Either the flow is captured well around the fibre bundle and the flow inside the bundle seems to be at a complete stand-still or the velocity field inside the bundle can be accurately described but the velocities outside the bundle are non-physical.

**RESULTS**

Initially, the velocity field was captured within the rectangular array. The velocity field is shown in Fig. 10.

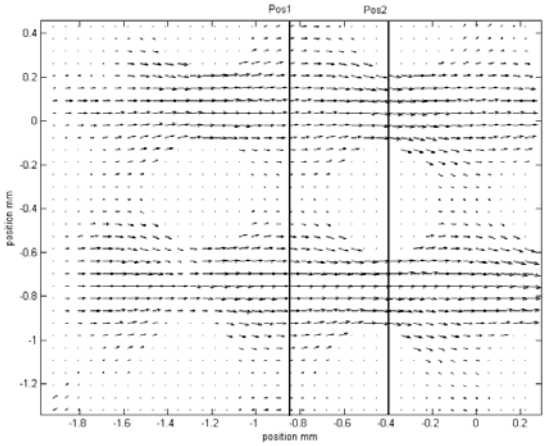


Fig.10 Velocity field in rectangular fibre array

There is limited movement between the rows of fibre although a circular motion can be observed. This is followed by a natural increase in velocity in the passage between fibres due to a decreasing cross-section area of the flow according to Fig. 11.

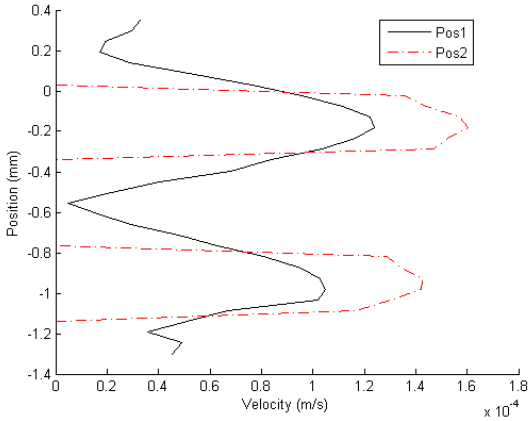


Fig.11 Velocity profiles for min and max cross-section area

Due to air entering the channel, an opportunity to investigate how disturbances in the fibre array affected the flow field materialized. Figure 12 shows how an air bubble was trapped between two fibres in the same row and Fig.13. shows how the bubble forced part of the flow to go into the overlying passage.

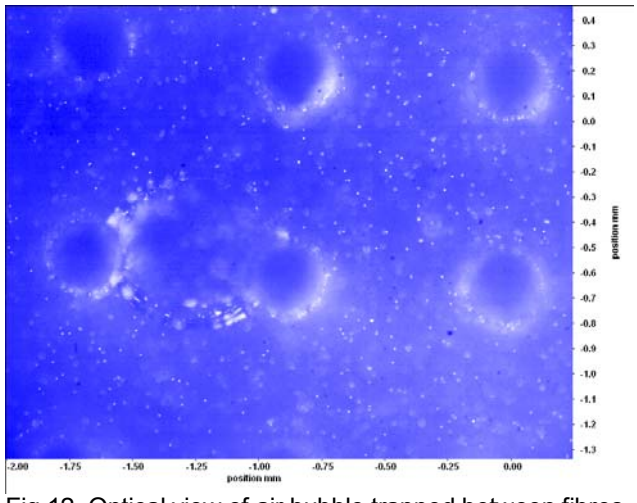


Fig.12 Optical view of air bubble trapped between fibres

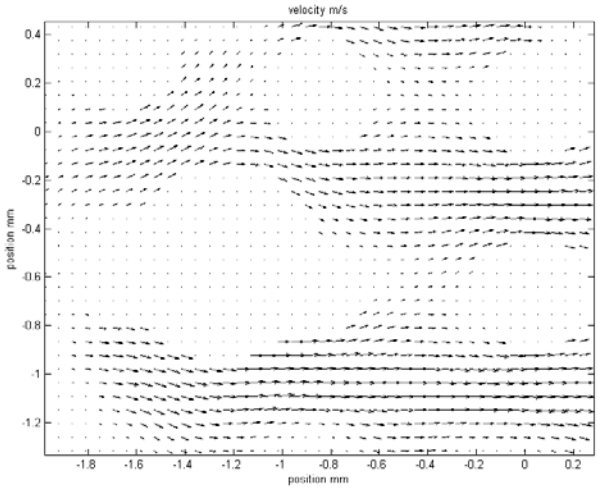


Fig.13 Velocity field for flow around air bubble in a rectangular fibre array

So far all the measurements were taken close to the bottom of the channel floor implying that there is very little fluid between the plane of measurement and the objective. For this case really high quality measurements can be achieved. This is exemplified in Figure 14 where the velocity field is captured within a hexagonally arranged array and the result is truly as one could expect.

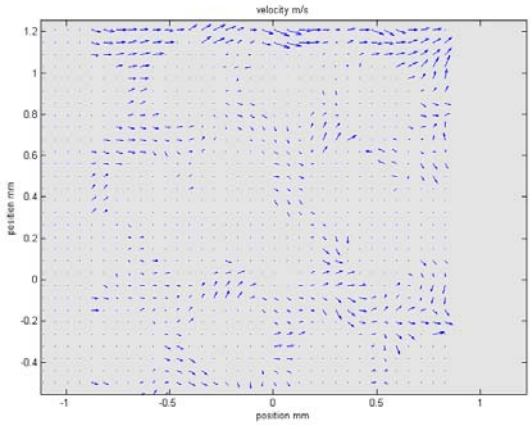


Fig.14. Velocity field near bottom of the channel.

As the measurement plane was moved deeper into the channel with a corresponding increase in the distance from the bottom plane a decrease in the optical quality of the pictures was noted. An easy way to reduce the background noise in these images is to average over the entire time-series and then subtracting that average from every image in the series. Fig.15. shows the velocity field obtained in the centre of the channel using that technique. Hence it has been demonstrated that the μPIV technique can be used to visualise the flow within an array of fibres, even far away from the edge of the cell being closest to the objective.

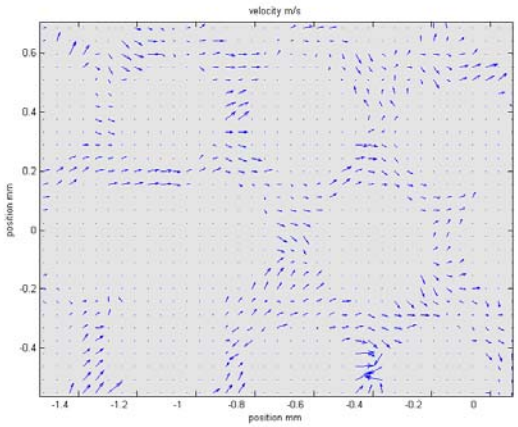


Fig.15. Velocity field near the middle the channel within the array.

An investigation was also made in which the flow around the fibre bundle was captured. In Figure 16, three fibres can be vaguely seen in the upper part of the plot. The velocity near the fibres is much lower than the bulk flow which makes it hard to visualize.

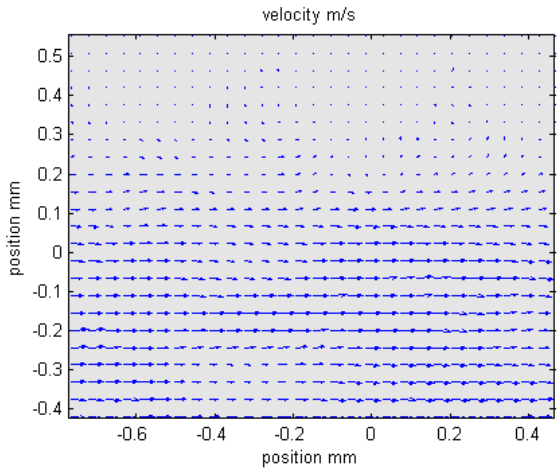


Fig.16. Velocity field near the middle the channel at the border of the array.

Some small disturbances in the velocity field can be observed but since PIV results are dependent on both the grid size and the statistical data obtained from several images, these could most likely be reduced by using a finer grid or a larger sample of images when doing the sum of correlations.

**CONCLUSIONS**

Modelling porous media flow using a combination of macro- and micro-scale techniques offers the possibility to model complicated geometries and obtain results which show the effect that the porous media has on the general flow. The Boundary Element Method is an excellent approach as far as the capture of the micro-scale details of the flow is concerned, in addition, the permeability results obtained from the BEM, could easily be used as input to the porous data used in FV/FE programs. It is finally shown that Micro Particle Image Velocimetry is a very promising technique for experimental observations as well as quantitative

derivations of such flow phenomena. The methodology here proposed should however be further developed and refined.

**ACKNOWLEDGEMENTS**
This work was partly financed by NANOFUN-POLY European network of excellence through SWEREA-SICOMP AB. The support of the US National Science Foundation, IREE program, was also of great importance.

**NOMENCLATURE**
R radius, m
K permeability, $m^2$
*f* fibre volume fraction
$\Phi_i$ inter-tow porosity
$N_f$ number of fibres
λ tow axis ratio
δ inter-fibre spacing, m

**REFERENCES**
Agelinchaab, M., Tachie, M.F. and Ruth, D.W. (2006): ''Velocity measurement of flow through a model three-dimensional porous medium''. *Physics of Fluids,* Vol. 18.

Blackford, L.S., Choi, J., Cleary, A., D'Azevedo, E., Demmel, J., Dhilllon, I., Dongarra, J, Hammarling, S., Henry, G., Stanley, K., Walker, D., Whaley, R.C. (1997): ''ScaLAPACK user's guide''. *SIAM,* Philadelphia.

Brebbia, C.A. and Dominguez, J. (1989): ''Boundary elements – an introductory course''. *McGraw-Hill*.

Chen, X. and Papathanasiou, T.D. (2007): ''Micro-Scale Modelling of Axial Flow through Unidirectional Disordered Fiber Arrays''. *Composites Science and Technology,* Vol. 67, pp. 1286-1293.

Chen, X. and Papathanasiou, T.D. (2008): ''The transverse permeability of disordered fiber arrays: A statistical correlation in terms of the mean interfiber spacing''. *Transport in Porous Media,* Vol. 71, pp. 233-251.

Gebart, B.R. (1992): ''Permeability of Unidirectional Reinforcements for RTM''. *Journal of Composite Materials,* Vol. 26, No. 8, pp. 1100-1133.

Larson, R.E. and Higdon, J.J.L. (1987): ''Microscopic flow near the surface of two-dimensional porous media: 2 Transverse flow''. *J. Fluid Mechanics,* Vol. 178, pp.

Lundstrom, T.S., Frishfelds, V. and Jakovics, A. (2004): ''A statistical approach to permeability of clustered fibre reinforcements''. *J. Compos. Mater.*, Vol. 38, pp. 1137–1149.

Meinhart, C.D., Wereley, S.T. and Gray, M.H.B. (2000): ''Volume illumination for two-dimensional particle image velocimetry''. *Meas. Sci. Technol.,* Vol. 11, pp. 809-814.

Nicolis, G. and Prigogin, I. (1989): ''Exploring complexity''. *W.H. Freeman & Company*, pp. 328.

Nordlund, M., Lundström, T.S., Frishfelds, V. and Jakovics, A. (2006): ''Permeability network model to non-crimp fabrics''. *Composites Part A*, Vol. 37A, pp. 826-835.

Parnas, R.S., Salem, A.J., Sadiq, T.A., Wang, H.P. and Advani, S.G. (1994): ''Interaction between micro- and macro-scopic flow in RTM performs''. *Compos. Struct.,* Vol. 27, pp. 93–107.

Patel, N. and Lee, L.J. (1995): ''Effects of fiber mat architecture on void formation and removal in liquid composite molding''. *Polym. Compos.,* Vol. 16, pp. 386–399.

Phelan, F.R. and Wise, G. (1996): ''Analysis of transverse flow in aligned fibrous porous media''. *Composite Part A,* Vol. 27, pp. 25-34.

Raffel, M., Willert, C. and Kompenhans, J. (1998): ''Particle Image Velocimetry; A Practical Guide''. *Springer-Verlag*.

Zhong, W.H., Currie I.G. and James, D.F. (2006): ''Creeping flow through a model fibrous porous medium''. *Experiments in Fluids,* Vol. 40, pp 119-126.